Numerical simulation of the gas mixing behavior in a soot conditioning system

G. Lindner[1], A. Nowak[2], S. Schmelter[1]

[1] Physikalisch-Technische Bundesanstalt (PTB), Abbestr. 2-12, 10587 Berlin, Germany
[2] Physikalisch-Technische Bundesanstalt (PTB), Bundesallee 100, 38116 Braunschweig, Germany
E-mail (corresponding author): gert.lindner@ptb.de

Abstract

In order to establish a primary soot aerosol standard for automotive exhaust measurements, a high-accuracy soot generator as well as a well-defined aerosol conditioning, dilution, and homogenization unit is needed. In this contribution, the mixing behavior of different gases under different junction conditions was numerically investigated to gain insight for favorable setup geometries and flow conditions of soot measuring systems. The overall goal was to find the design that leads to the fastest mixing of the different incoming gas components for a given pipe length. For this purpose, a main pipe with two symmetrically arranged side inlet pipes was considered, where the angle of inclination of the side pipes as well as the inflow conditions were varied. It was found that, in general, the required pipe length to reach a sufficiently homogeneous gas mixture decreases with increasing inclination angles exhibiting the best performance at obtuse angles. Furthermore, it has been observed that the turbulent Schmidt number used in the turbulence modeling of the transport equation of the mass fraction of aerosol-laden gas has an important influence on the speed of mixing. In general one can say that, the smaller the turbulent Schmidt number, the faster the mixing. Nevertheless, it can also be observed that the qualitative behavior how the mixing length in- or decreases with changes in the geometry is invariant under different turbulent Schmidt numbers.

1. Introduction

At the national metrological institute of Germany (PTB) a new aerosol standard and conditioning unit for dilution was proposed, realized by [1] and characterized by the working group of aerosol and particle diagnostic [2]. The main parts of the calibration infrastructure encompass a specially modified HiMass-CAST soot generator [3]. Such high accuracy soot generators need also well-defined aerosol conditioning, dilution and homogenization process steps in order to vary, e.g., the particle number concentration over the legally relevant range. The high accuracy required for a primary soot standard also asks for new approaches to mix, dilute and homogenize the generated soot aerosol, with selective influence on particle shape and size distribution.

Accompanying computational fluid dynamics (CFD) studies were performed to generate an inside view of the gas-flow-soot-aerosol interaction process. The spatial soot aerosol distribution in the conditioning section of the flow channel is affected by the turbulence of the carrier fluid.

The RANS (Reynolds-averaged Navier–Stokes equations) model for turbulent flows with mass transfer generally estimates the turbulent scalar flux assuming the gradient diffusion hypothesis, which requires definition of the turbulent Schmidt number. The turbulent Schmidt number $\mathrm{Sc_t}$ has an important influence on the speed of mixing and appears in all scalar transport equations which used a gradient type description to model diffusion. To see this dependency in our application $\mathrm{Sc_t}$ is varying.

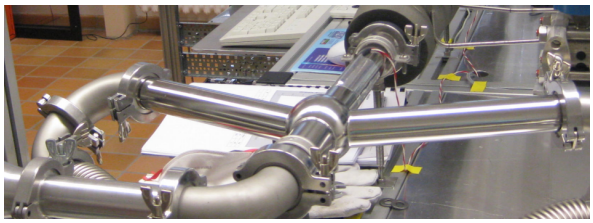

Figure 1: Construction of the aerosol dilution- and conditioning unit.

By means of a regression model the collected data of alltogether 160 cases is combined so that the mixing capability can also be predicted for other parameter combinations.

The paper is organized as follows: Section 2 is subdivided. At first the geometry of the measurement configuration is introduced and the numerical scheme used for the CFD simulation with ANSYS CFX® is sketched. The considered turbulence models are described as well as the impact of the turbulent Schmidt number. Simulation results are presented in Section 3. Finally, conclusions are drawn in Section 4.

2. Modeling the Multiple Inlet System

The considered flow region consists of a main pipe with a diameter d of 0.0377 m and two symmetrically arranged identical side pipes as shown in Figure 1. Such geometries are used in soot measuring systems, where an aerosol-laden air flow is mixed with pure air flows [1]. In

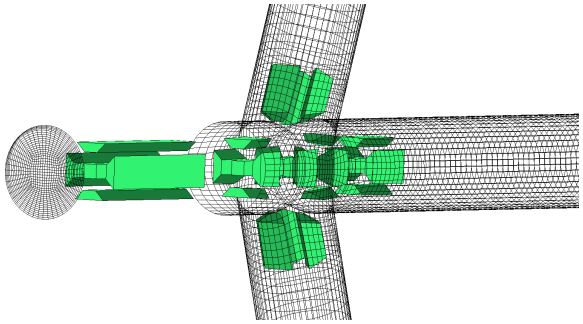

Figure 2: Sketch of the mixing section of the hexahedral mesh used for the numerical simulations. A coarsen pre-mesh including the block structure (green) is shown.

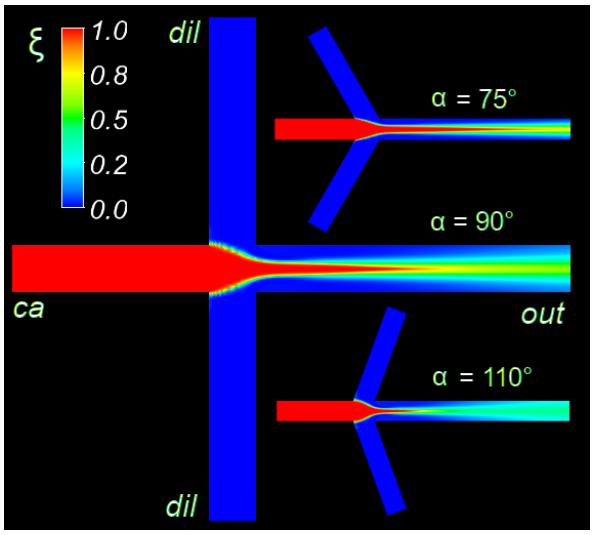

Figure 3: Contour plots of the mass fraction ξ in ZY-plane for FC5, i. e., $\mathrm{Re} = 30960$ and $\xi_\infty = 0.5$ for three different angles of inclination, $\alpha = 75°$, $90°$, and $110°$. The flow direction is from left to right.

this contribution, we generally refer to the presentation given in [4]. Specifically the case where the mixing chamber is not enclosed by a sphere is of our interest. For the numerical simulation, the whole three-dimensional geometry has been meshed with hexahedral elements using the mesh generation tool ICEM/CFD-Hexa. An impression is given in Figure 2. For details concerning mesh generation and a grid refinement study we also refer to [4]. In the numerical simulations, the angle of inclination α between the main pipe from ca and the two side pipes dil was varied in a dedicated range as shown in Figure 3. The following eight angles of inclination are considered, namely $\alpha = 60°$, $75°$, $90°$, $100°$, $110°$, $115°$, $120°$, and $130°$. Five different inflow conditions are investigated, where flow rates in the main and side pipes vary between 50 and 400 l/min, for details see Table 1. Using the magnitude of the velocity profile at the outlet, the Reynolds number Re varies between 7740 for FC1 and 30960 for FC5.

Table 1: Volume flow rates at the inlets. Q_{ca} at the main inlet, Q_{dil} equal portions at side inlets and corresponding Reynolds Re

case	$Q_{ca} + 2 \cdot Q_{dil}$	$frac$	ξ_∞	$\mathrm{Re_{ch}}$
FC1	100 + 2 × 50	1/2 + 1/2	0.50	7740
FC2	200 + 2 × 50	2/3 + 1/3	1/3	11610
FC3	300 + 2 × 100	3/5 + 2/5	0.40	19350
FC4	400 + 2 × 100	2/3 + 1/3	1/3	23220
FC5	400 + 2 × 200	1/2 + 1/2	0.50	30960

2.1. Governing Equations

The gas flow in the cross pipe system is assumed to be in steady-state and incompressible. The corresponding Navier-Stokes equations model the conservation of mass and momentum and are given by

$$\nabla \cdot \boldsymbol{u} = 0\,, \qquad \boldsymbol{u} \cdot \nabla \boldsymbol{u} = -\frac{1}{\rho}\nabla p + \nu \nabla^2 \boldsymbol{u}, \qquad (1)$$

where $\boldsymbol{u}$ is the velocity, p the pressure and ν the kinematic viscosity. Standard no-slip boundary conditions on the walls and a zero-gradient boundary condition at the outlet out is applied. In the pipe system, we distinguish the gas originating from the inlet of the side pipes (pure air) from the one coming from the main pipe (air with soot particles) only by means of a marker. Thus, we have only one additional equation modeling the transport of the mass fraction ξ

$$\boldsymbol{u} \cdot \nabla \xi = \nabla \cdot (D_\xi \nabla \xi), \qquad (2)$$

where D_ξ is the diffusion coefficient. Note that this modeling approach can be used, since the volume fraction of soot particles in the considered system is in the order of 10^{-7} and hence it can be assumed that the particles do not have any influence on the flow, see, e. g., [5,6]. Hence, the incoming gas at the three inlets (of the main pipe and of the two side pipes) is taken to be air at room temperature. The mass fraction ξ is equal to 0 at the side inlets dil and 1 at the inlet of the main pipe ca. The volume flow rate at the main inlet ca is denoted by Q_{ca} and the flow rate at both side inlets by Q_{dil}. Then the ratio of the side inlet gas far behind the pipe junction is expected to approach ξ_∞ with

$$\xi_\infty = 2 \cdot Q_{dil}/(Q_{ca} + 2 \cdot Q_{dil}). \qquad (3)$$

For a sufficiently long pipe, we expect a homogenous gas mixture, i. e., $\xi(x, y, z) \approx \xi_\infty$ for all x, y and sufficiently large z. Thus, we call ξ_∞ the *homogeneous equilibrium mass fraction*.

2.2. Turbulence Closure Schemes

Current engineering CFD simulations are largely built on linear eddy-viscosity turbulence models. Turbulence is modeled by Reynolds-averaging (RANS method). The arising closure problem is solved by introducing additional transport equations, usually for the turbulent

kinetic energy k and for either the energy dissipation rate ϵ (k-ϵ models) or the turbulent frequency ω (k-ω models). There exist a lot of turbulence models, which are based on these two basic models (or on combinations of them). A more sophisticated approach to solve the closure problem is to model the different terms of the Reynolds stress tensor separately. This leads to the family of Reynolds stress models. These models usually also have an additional transport equation for either ϵ (ϵ-based models) or ω (ω-based models). Further information on turbunce modeling can be found in [7].

In this contribution, several turbulence models have been investigated for the considered application. The results revealed that ω-based models are much more suitable for this problem than ϵ-based models. Thus, results are only shown for the Shear Stress Transport (SST) model by Menter [8] as well as for the more advanced ω-based Baseline Reynolds Stress Model (BSL-RSM) [9]. These findings are in agreement with [10], where the turbulent and thermal mixing in T-junctions was investigated. There it was stated that the results obtained by the ω-based turbulence models (standard k-ω and SST) are in better agreement with experimental data than those obtained by the realizable k-ϵ model. In [11] several ω-based turbulence models were compared with experimental data. There, it was shown that both, the SST model as well as the BSL-RSM satisfactorily predicted the turbulent mixing.

2.3. About turbulent Schmidt number $\mathrm{Sc_t}$

After applying the RANS approach the averaged transport equation for the mass fraction reads (note that u and ξ denote Reynolds-averaged quantities in the following)

$$\boldsymbol{u} \cdot \nabla \xi = \nabla \cdot \left(\left(D_\xi + \frac{\nu_t}{\mathrm{Sc_t}} \right) \nabla \xi \right), \qquad (4)$$

which contains the turbulent viscosity ν_t and the turbulent Schmidt number $\mathrm{Sc_t}$. Usually it is assumed, that the turbulent Schmidt number is $\mathrm{Sc_t} \sim 0.9$, see, e.g., [12, 13]. The authors of [14] recommend for RANS modeling, particularly when the k-ω shear stress transport (SST) model is employed, a turbulent Schmidt number less than 0.85. In [15] a value of $\mathrm{Sc_t} = 0.5$ is proposed for *free turbulence* and $\mathrm{Sc_t} = 0.9$ for tube flow. In [10,11,16], where the turbulent and thermal mixing in a T-junction was investigated, the turbulent Schmidt number was varied in the range $0.1 \leq \mathrm{Sc_t} \leq 0.9$. There, a much smaller Schmidt number $\mathrm{Sc_t} = 0.2$ was found to fit best the experimental data for the considered configuration. In [12] it is stated that no universal value of $\mathrm{Sc_t}$ has been established and empirical values have been used in different studies. Furthermore, it was confirmed that the value of $\mathrm{Sc_t}$ has large influence on the prediction of the accuracy of mass transfer. Thus, the influence of different turbulent Schmidt numbers is investigated in this contribution. Taking the literature into account, we decided to compare $\mathrm{Sc_t} = 0.2$ and $\mathrm{Sc_t} = 0.8$ in this study.

2.4. Mixing Performance

In the following, we are interested in the downstream evolution of the mixing for the different geometries. In order to estimate the homogeneity of the involved gas streams, a possible adaptation of the 'intensity of segregation' concept by Danckwerts [17] can be used, see [18, 19]. In Equation (5) we introduce the intensity of segregation I_s as the normalization of the variance by its maximum value

$$I_s(z) = \frac{\sigma^2(z)}{\sigma^2_{max}(z)} \quad \text{with} \quad \sigma^2_{max}(z) = \sigma^2(z=0),$$
$$\sigma^2(z) = \frac{1}{|A|} \int_A \left(\xi(x,y,z) - \overline{\xi}(z) \right)^2 dA\,. \qquad (5)$$

This implies integrating the mass fraction over the surface area of a cross plane $|A|$ respectively $\forall z$ where $\overline{\xi}(z)$ denotes the mean value of mass fraction and $\sigma^2_{max}(z)$ is the maximum possible variance given at the entrance. Since I_s is normalized, an intensity value of 1 corresponds to complete segregation, whilst a value of 0 indicates perfect mixing. Furthermore, a threshold level $I_{sl} = \frac{1}{10}$ is fixed. If a smaller threshold level has to be considered, longer downstream distances than 1.43 m are required. Then, we define the mixing length $l_m(I_{sl})$ as the smallest value of z for which the condition

$$I_{sl} \leq I_s(x,y,z) \qquad (6)$$

is satisfied $\forall x, y$. For further details, we refer to [4].

3. Results

We have carried out systematic simulations for each of the five flow conditions varying the angles between the main pipe and the symmetrically arranged side inlets in the range between 60° and 130°. Furthermore, we have investigated two different turbulent Schmidt numbers ($\mathrm{Sc_t} = 0.2$ and $\mathrm{Sc_t} = 0.8$) and different turbulence models.

3.1. Mixing Quality

For the description of the mixing quality, the intensity of segregation was determined for different flow regimes to assess the quality of the mixing process along the channel. The development of the mass fraction ξ in an axial view is presented in Figure 3. As expected, for large z, the quantity ξ approaches a homogeneous distribution. In case of obtuse angles such a homogenization is reached earlier leading to shorter mixing lengths. Figure 4 shows the dependency of I_s on the angle α for FC5, which corresponds to $\mathrm{Re} = 30960$ and $\xi_\infty = 0.5$. One observes that the smaller the angle, the slower the decrease of I_s. This means that the mixing quality improves with larger angles α. Best mixing is obtained for obtuse angles for the multiple inlet system. Note that the results shown in Figure 4 have been obtained by applying the BSL-RSM turbulence model and using a value of 0.8 for the turbulent

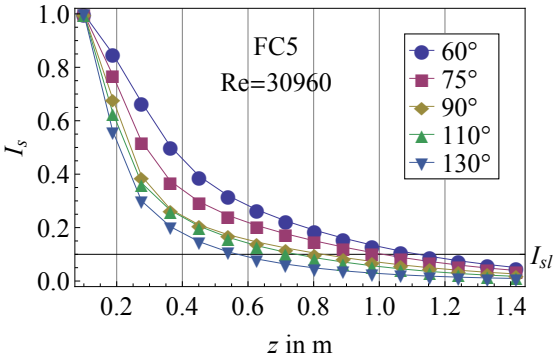

Figure 4: Angle dependence of I_s for FC5, i. e., Re $= 30960$ and $\xi_\infty = 0.5$, for selected geometries, namely $\alpha = 60°, 75°, 90°, 110°$ and $130°$ computed with BSL-RSM model and for a turbulent Schmidt number $\mathrm{Sc_t} = 0.8$. The threshold level I_{sl} is marked at which the mixing length is obtained.

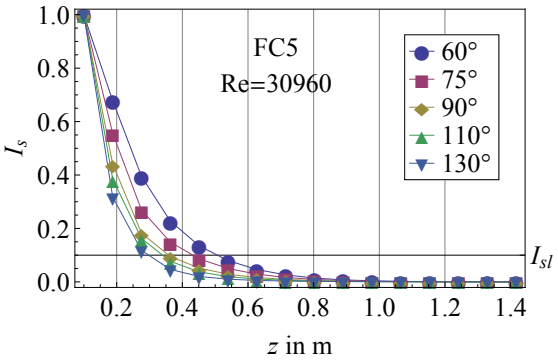

Figure 5: The same as shown in Figure 4 but for a turbulent Schmidt number $\mathrm{Sc_t} = 0.2$.

Schmidt number. Analoguous results for the SST model are presented in [4], where also a more detailed discussion of the results can be found. The results for the BSL-RSM and for the SST model are very similar.

In this study, several turbulence models have been tested. The results can be summarized as follows:

- k-ω-based models are much more suitable for the considered application than k-ϵ-based models.
- In general, the more advanced Reynolds stress models do not lead to better results. Those models are only suitable if they are ω-based.
- The three tested ω-based models (standard k-ω, SST, and BSL-RSM) lead to similar results.

3.2. Influence of $\mathrm{Sc_t}$

Figure 5 shows as Figure 4 the dependency of I_s on the angle α for FC5. However, a much smaller turbulent Schmidt number $\mathrm{Sc_t} = 0.2$ has been used. This leads to a faster mixing and thus to a drastically shortening of the mixing lengths in all cases. For $\alpha = 130°$, for example, the mixing length decreases from about 0.55 m for $\mathrm{Sc_t} = 0.8$ to 0.275 m, i. e., it is halved. For smaller angles, the mixing lengths reduce even more. However,

Table 2: Coefficients of the regression model, see Equation (7).

a_0	a_1	a_2	a_3	a_4
1.2249	-0.4292	-2.9561	-0.3867	0.1127

a_5	a_6	a_7	a_8	a_9
3.5623	-0.0329	0.0331	3.7105	-0.9067

Table 3: Mean square error σ_{est} (residuals) for regression.

	$\mathrm{Sc_t} = 0.8$	$\mathrm{Sc_t} = 0.2$
σ_{est}	0.02603	0.00905

the qualitative behavior (namely the order of the curves) is preserved. In order to determine the right mixing lengths for this application, the results have to be compared with experimental data so that the value of the turbulent Schmidt number that is appropriate can be determined.

In order to derive a general expression of the mixing length l_m as a function of parameters α, ξ and $\mathrm{Sc_t}$, the following ansatz is used:

$$\begin{aligned} l_m(\alpha, \xi_\infty, \mathrm{Sc_t}) = \\ a_0 + a_1\alpha + a_2\xi_\infty + a_3\mathrm{Sc_t} + a_4\alpha^2 + a_5\xi_\infty^2 \\ + a_6\alpha\xi_\infty + a_7\alpha\mathrm{Sc_t} + a_8\xi_\infty\mathrm{Sc_t} + a_9\alpha\xi_\infty\mathrm{Sc_t}. \end{aligned} \quad (7)$$

Here, α denotes the angle of inclination in radians. The coefficients a_i, $i = 0, \ldots, 9$, are determined by solving the regression problem for the 2×80 data points. Such a set of 80 data points is given by the combination of the five flow cases FC1, ..., FC5 (corresponding to $\xi_\infty \in \{1/3, 0.4, 1/2\}$), the two different turbulent Schmidt numbers $\mathrm{Sc_t} \in \{0.2, 0.8\}$, and the eight different angles $\alpha \in \{\pi/3, 5\pi/12, \pi/2, 5\pi/9, 11\pi/18, 23\pi/36, 2\pi/3, 13\pi/18\}$. We used two data sets, one obtained by calculation with the SST model, and one with BSL-RSM. The resulting coefficients are summarized in Table 2. Figure 6 shows the results of the numerical simulations for 160 different cases as well as the regression curves evaluated for the three different values of ξ_∞ and two different values of $\mathrm{Sc_t}$. Note that we have chosen Equation (7) as regression model because its mean square error is significantly smaller than for the linear model. Although higher order models give even smaller errors, we rejected them because of their unphysical oscillations.

To determine the quality of the fit for these cases, we define σ_{est} as the mean square error given by

$$\sigma_{est} = \left(\frac{\sum (l_m^{sim} - l_m)^2}{N} \right)^{1/2}, \quad (8)$$

where l_m^{sim} are the data points from the simulation, l_m are the calculated ones from the regression, and $N = 5 \times 8 \times 2 \times 2$ is the number of pairs in the data set given. The resulting residuals are given in Table 3.

Equation (7) can also be used to predict the mixing length for other parameter combinations. Figure 7 shows

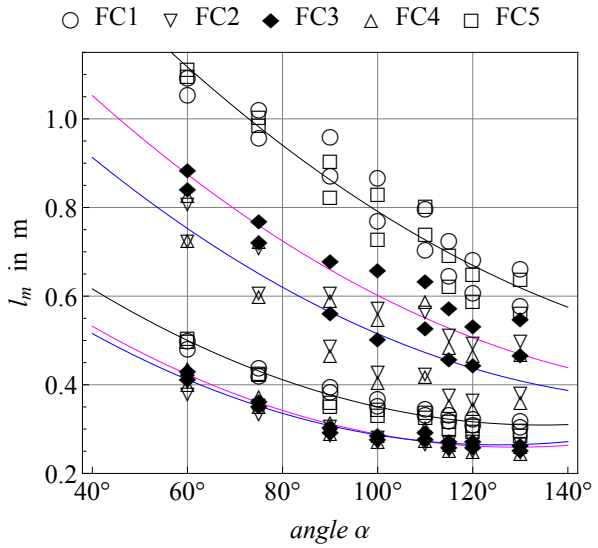

Figure 6: Mixing length as a function of angle of inclination α evaluated for the three different values of ξ_∞ (black: $\xi_\infty = 0.5$, pink: $\xi_\infty = 0.4$, blue: $\xi_\infty = 1/3$) and the two different values of $\mathrm{Sc_t}$ respectively. The three top curves with $\mathrm{Sc_t} = 0.8$, the three bottom curves with $\mathrm{Sc_t} = 0.2$.

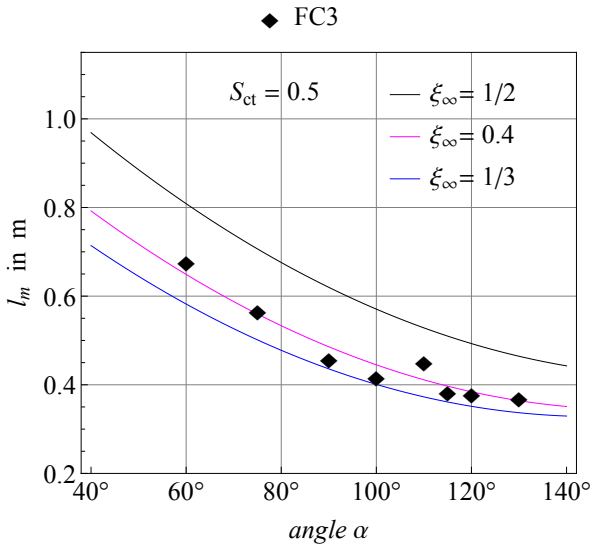

Figure 7: Predicted mixing length l_m as a function of angle of inclination α for the three different values of ξ_∞ (black: $\xi_\infty = 0.5$, pink: $\xi_\infty = 0.4$, blue: $\xi_\infty = 1/3$) for $\mathrm{Sc_t} = 0.5$. Subsequent selected simulation values are added.

the three curves one obtains for the $\xi_\infty = 0.5$, $\xi_\infty = 0.4$, and $\xi_\infty = 1/3$, respectively, for the turbulent Schmidt number $\mathrm{Sc_t} = 0.5$.

In order to check the quality of the regression model, we compare this prediction for $\mathrm{Sc_t} = 0.5$ with simulation results obtained by the SST model for FC3. The black diamonds in Figure 7 mark the simulated values of l_m. One can see that the simulated and predicted values match quite well. The error of this prediction is less than 1%.

4. Conclusion

In this contribution, the mixing behavior of different gases under different junction conditions was numerically investigated to gain insight for favorable setup geometries and flow conditions of soot measuring systems. The overall goal was to find the design that leads to the fastest mixing of the different incoming gas components for a given pipe length. For this purpose, we considered the same set-up as in [4], namely a main pipe with two symmetrically arranged side inlet pipes, where the angle of inclination of the side pipes was varied. However, in this study, the main focus was on the investigation of the influence of using different turbulence models and different values for the turbulent Schmidt number.

A comparison of different turbulence models showed that ω-based models are much more appropriate for the considered application than ϵ-based ones. The three tested ω-based models (standard k-ω, SST, and BSL-RSM) lead to very similar results.

On the other hand, the turbulent Schmidt number has a much bigger influence on the resulting mixing lengths. In general one can say that, the smaller the turbulent Schmidt number, the faster the mixing. Nevertheless, it can also be observed that the qualitative behavior how the mixing length decreases with increasing angle is invariant under different turbulent Schmidt numbers.

Furthermore, a regression model, which combines 160 simulated cases, has been introduced in Equation (7). It was shown that this model can be used to predict the mixing length also for other parameter combinations. The prediction for $\mathrm{Sc_t} = 0.5$ has been validated by comparison with additional CFD simulations for FC3. The results show good agreement.

Acknowledgement

Parts of this work have been funded by cooperative projects with the German Garage Equipment Association (ASA) and within the European Metrology Research Programme (EMRP) in ENV02 PartEmission. The authors would like to gratitude André Fiebach for his assistance and for fruitful discussion.

Bibliography

[1] A. Nowak, G. Lindner, A. Jordan-Gerkens, N. Böse, and V. Ebert. Developing a National Standard for Soot Mass Concentration and Opacity at PTB in Germany. In *16th ETH-Conference on Combustion Generated Nanoparticles, Zurich, Switzerland*, 2012.

[2] A. Kuntze, M. Hildebrandt, A. Nowak, A. Jordan-Gerkens, D. Bergmann, E. Buhr, and V. Ebert. Characterization of a PTB-Standard for Particle Number Concentration of Soot Particles. In *18th ETH-Conference on Combustion Generated Nanoparticles, Zurich, Switzerland*, Zurich, 2014.

[3] L. Jing. Standard Combustion Aerosol Generator (SCAG) for Calibration Purposes. In *3rd*

ETH Workshop Nanoparticle Measurement, Zurich, Switzerland, August 1999.

[4] G. Lindner, S. Schmelter, R. Model, A. Nowak, V. Ebert, and M. Bär. A computational fluid dynamics study on the gas mixing capabilities of a multiple inlet system. *J. Fluids Eng*, 138(3), 2015.

[5] S. Elgobashi. Particle-Laden Turbulent Flows: Direct Simulation and Closure Models. *Appl. Sci. Res.*, 48(301-314), 1991.

[6] S. Elgobashi. On Predicting Particle-Laden Turbulent Flows. *Appl. Sci. Res.*, 52(309-329), 1994.

[7] D.C. Wilcox. *Turbulence Modeling for CFD*. DCW Industries, 3rd edition, November 2006.

[8] F. R. Menter. Two-Equation Eddy-Viscosity Turbulence Models for Engineering Applications. *AIAA Journal*, 32(8):1598–1605, 1993.

[9] Inc. ANSYS. ANSYS CFX User Manual, November 2012.

[10] M. Aounallah, M. Belkadi, L. Adjlout, and O. Imine. Thermal Mixing Length Determination by RANS Models in T-Junction. In *ASME 2010 10th Biennial Conference on Engineering Systems Design and Analysis*, volume 3, pages 369–376, Istanbul, Turkey, July 2010. ASME.

[11] Th. Frank, C. Lifante, H.-M. Prasser, and F. Menter. Simulation of Turbulent and Thermal Mixing in T-junctions Using URANS and Scale-Resolving Turbulence Models in ANSYS CFX. *Nuclear Engineering and Design*, 240(9):2313 – 2328, 2010. Experiments and CFD Code Applications to Nuclear Reactor Safety (XCFD4NRS).

[12] Yoshihide Tominaga and Ted Stathopoulos. Turbulent Schmidt Numbers for CFD Analysis with Various Types of Flowfield. *Atmospheric Environment*, 41(37):8091 – 8099, 2007.

[13] A. R. Paschedag. *CFD in der Verfahrenstechnik: Allgemeine Grundlagen und Mehrphasige Anwendungen*. Wiley-VCH, Weinheim, 2004.

[14] J. Ling, C. Elkins, and J. Eaton. Optimal Turbulent Schmidt Number for RANS Modeling of Trailing Edge Slot Film Cooling. *J. Eng. Gas Turbines Power*, 137(7), 2015.

[15] R. B. Bird, W. E. Stewart, and E. N. Lightfoot. *Transport Phenomena, R. B. Bird, W. E. Stewart, and E. N. Lightfoot, John Wiley and Sons, Inc., New York (1960). 780 pages.*, volume 7. American Institute of Chemical Engineers, 1961.

[16] J.B.W. Kok and S. van der Wal. Mixing in T-junctions. *Applied Mathematical Modelling*, 20(3):232–243, 1996.

[17] P.V. Danckwerts. The Definition and Measurement of some Characteristics of Mixtures. *Applied Scientific Research, Section A*, 3(4):279–296, 1952.

[18] D. Bothe, C. Stemich, and H. J. Warnecke. Fluid Mixing in a T-shaped Micro-Mixer. *Chemical Engineering Science*, 61(9):2950–2958, 2006.

[19] J. Aubin, D.F. Fletcher, J. Bertrand, and C. Xuereb. Characterization of the Mixing Quality in Micromixers. *Chem. Eng. Technol.*, 26:1262–1270, 2003.